pubs.acs.org/Biomac

Article

Fingolimod-Conjugated Charge-Altering Releasable Transporters Efficiently and Specifically Deliver mRNA to Lymphocytes In Vivo and In Vitro

Stefano Testa, Ole A. W. Haabeth, Timothy R. Blake, Trevor J. Del Castillo, Debra K. Czerwinski, Ranjani Rajapaksa, Paul A. Wender, Robert M. Waymouth, and Ronald Levy*

Cite This: https://doi.org/10.1021/acs.biomac.2c00469

Read Online

ACCESS | Metrics & More | Article Recommendations | Supporting Information

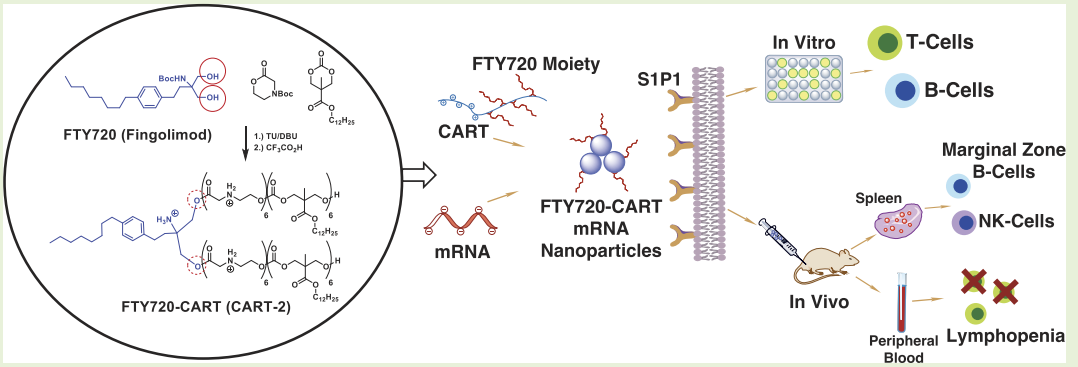

ABSTRACT: Charge-altering releasable transporters (CARTs) are a class of oligonucleotide delivery vehicles shown to be effective for delivery of messenger RNA (mRNA) both in vitro and in vivo. Here, we exploited the chemical versatility of the CART synthesis to generate CARTs containing the small-molecule drug fingolimod (FTY720) as a strategy to increase mRNA delivery and expression in lymphocytes through a specific ligand−receptor interaction. Fingolimod is an FDA-approved small-molecule drug that, upon in vivo phosphorylation, binds to the sphingosine-1-phosphate receptor 1 (S1P1), which is highly expressed on lymphocytes. Compared to its non-fingolimod-conjugated analogue, the fingolimod-conjugated CART achieved superior transfection of activated human and murine T and B lymphocytes in vitro. The higher transfection of the fingolimod-conjugated CARTs was lost when cells were exposed to a free fingolimod before transfection. In vivo, the fingolimod-conjugated CART showed increased mRNA delivery to marginal zone B cells and NK cells in the spleen, relative to CARTs lacking fingolimod. Moreover, fingolimod-CART-mediated mRNA delivery induces peripheral blood T-cell depletion similar to free fingolimod. Thus, we show that functionalization of CARTs with a pharmacologically validated small molecule can increase transfection of a cellular population of interest while conferring some of the targeting properties of the conjugated small molecule to the CARTs.

INTRODUCTION

In the last decade, messenger RNA therapeutics have emerged as a promising new modality for the development of new vaccines, protein replacements, and gene-editing therapies.[1,2] The widespread administration of mRNA vaccines against SARS-CoV2[3−5] has highlighted the potential of gene therapies mediated by non-viral nanoparticle (NP) technologies, such as lipid NPs (LNPs).[6−8] Despite the success of current LNP technologies for gene delivery, the full potential of gene therapeutics will only be realized with the further development of technologies that can selectively deliver the gene of interest to specific cells and tissues in vivo.[1]

The modification of NP delivery systems with biological or small-molecule targeting ligands is one approach that has been used to direct gene delivery to specific cells or organs, sometimes referred to as active targeting.[1,9−11] Alternatively, recent studies have shown that the manipulation of the physicochemical properties of NP delivery systems (such as size, surface charge, and shape) can direct gene delivery to particular classes of cells or organs upon systemic administration in vivo, referred to as passive targeting;[1,10,11] nevertheless, the factors responsible for these effects are unclear and remain areas of active investigation. Understanding the rules for applying both of these strategies and their

Received: April 11, 2022
Revised: June 13, 2022

interplay is a critical step in realizing selective gene delivery in vivo.

We have previously reported a new class of amphiphilic oligomeric gene delivery vectors, charge-altering releasable transporters (CARTs), for mRNA delivery in cell culture and in vivo.[12] CARTs spontaneously form NPs upon simple mixing with oligonucleotides or other polyanionic cargos, and CART/mRNA NPs were shown to be effective in pre-clinical studies of vaccines for cancer[13,14] and SARS-CoV2.[15] The modular and efficient synthesis of the CART amphiphiles (eq 1)[12,16]

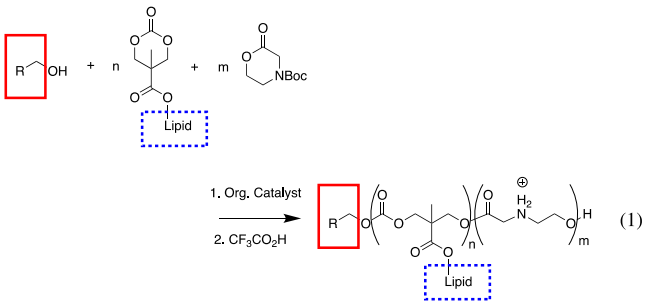

(1)

enabled studies that showed that the nature of the pendant lipid could influence the types of cells that were transfected efficiently. CARTs containing unsaturated lipids exhibited up to 80% transfection of EGFP RNA to lymphocytes.[17]

In mice, systemic administration of firefly luciferase (FLuc) mRNA with CARTs in vivo results in a selective Fluc expression in the spleen,[12,15,17,18] rather than the liver.[19] For CARTs bearing a saturated $C_{12}H_{25}$ lipid and *N*-hydroxyethyl glycine repeating units (D13/A11), the CART-RNA NPs were observed primarily in monocytes and dendritic cells in the spleen, with a lower uptake observed in B cells and T cells.[14]

As selective in vivo gene delivery to lymphocytes is a promising approach to many immunotherapies,[20] we sought to leverage the synthetic versatility of the CART platform to enhance mRNA delivery to lymphocytes in vivo through an active targeting approach. As the CART amphiphiles can be generated from a variety of alcohol initiators (eq 1), we targeted FTY720 (fingolimod), a small-molecule drug approved by the FDA for treatment of patients with multiple sclerosis. FTY720 acts as a validated agonist for the sphingosine-1-phosphate receptor 1 (S1P1), highly expressed on T cells and B cells in secondary lymphoid organs, causing prolonged internalization of the receptor and decreased efflux of lymphocytes into the bloodstream, leading to significant lymphopenia, which is at least in part responsible for the immunosuppressive effects of FTY720 in multiple sclerosis.[21−23]

Herein, we report a new class of CARTs incorporating FTY720 as an integral structural component of the CART as a strategy to enhance the in vivo delivery of mRNA to T cells and B cells by exploiting a specific S1P1 interaction. We demonstrate that CARTs incorporating FTY720 show enhanced transfection in cells expressing S1P1 both in cell culture and in vivo and that this enhanced transfection is abrogated upon pre-treatment with FTY720 in vitro. The FTY720-CARTs exhibit enhanced in vivo mRNA delivery to B cells and NK cells in the spleen upon IV injection relative to CARTs lacking FTY720. Moreover, the FTY720-CARTs, when administered IV, induce peripheral T-cell depletion analogous to that exhibited by FTY720 administration. These findings demonstrate that CART vectors are amenable to active targeting strategies for gene delivery applications and further suggest opportunities to utilize CARTs for the delivery of conjugated small-molecule drugs and to provide concomitant delivery of a conjugated small-molecule drug alongside a nucleic acid cargo.

MATERIALS AND METHODS

CART Synthesis and Characterization. **CART-1** (Bn-$D_{13}A_{11}$), the *N*-boc morpholinone, and MTC-dodecyl monomers were synthesized as previously reported (Mn(GPC) = 6000 Da $Đ$ = 1.25).[17] **CART-2** (FTY720-$D_{12}A_{12}$) was prepared by a slight modification of this procedure. In a nitrogen-filled glovebox, *N*-Boc morpholinone (21.5 mg, 0.1 mmol, 10.9 equiv) is dissolved in toluene (50 μL). To this solution are added a thiourea catalyst (TU, 1.8 mg, 0.005 mmol, 0.5 equiv), diazabycycloundecene (DBU, 0.78 mg, 0.005 mmol, 0.5 equiv), and an *N*-Boc-protected FTY720 initiator (4 mg, 0.01 mmol, 1 equiv) as a solution in 50 μL of toluene. The reaction was stirred for 2.5 h, and then MTC-dodecyl was added as a solid (35 mg, 0.1 mmol, 10.9 equiv). The reaction mixture was allowed to stir for an additional 1.5 h. The reaction was removed from the glovebox and quenched with 100 μL of acetic acid. The crude mixture is dialyzed overnight in (DCM/MeOH, 3.5 kDa M.W, cut-off). An aliquot of the protected material is subjected to size-exclusion gel permeation chromatography (Mn(GPC) = 9700 Da, $Đ$ = 1.20). The concentration after dialysis afforded 21 mg of clear residue, which was deprotected with 10% trifluoroacetic acid (TFA) in dry DCM (v/v, 2.1 mL, stirred for 4 h at RT and collected by rotary evaporation). The end-group analysis of the protected polymer by ^{1}H NMR showed 12 dodecyl carbonate units and 12 cationic aminoester units per FTY720 initiator.

CART-3 (**B-DMPA-$A_{11}D_{11}$**) and **CART-4** (**PhDEA-$A_{14}D_{14}$**) were prepared by the same method as **CART-2** with the substitution of benzyl-2,2-bis(hydroxymethyl)propionate (B-DMPA) or *N*-phenyldiethanolamine (PhDEA) in place of the *N*-Boc protected FTY720 initiator, respectively. Additional details are provided in the Supporting Information.

Mice and Cell Lines. 6 to 8 week old female BALB/c mice were purchased from the Charles River Laboratory and housed in the Laboratory Animal Facility of the Stanford University Medical Center (Stanford, CA). All experiments were approved by the Stanford Administrative Panel on Laboratory Animal Care and conducted in accordance with Stanford University Animal Facility and NIH guidelines. Jurkat cells (ATCC no. TIB-152) and K562 cell lines (ATCC no. CCL-243) were obtained from ATCC. CHO cells (Chinese hamster ovary) were obtained from the Levy lab inventory. Mycoplasma testing of cell lines was performed at 3 month intervals using a MycoAlert Detection Kit (Lonza). Jurkat and K562 cells were maintained in RPMI medium 1640 with L-glutamine (cCellgro; Corning) supplemented with 10% heat-inactivated FCS (HyClone), 1% penicillin/streptomycin (Gibco), and 50 μM of 2-mercaptoethanol (Gibco) to obtain the complete medium. CHO cells were maintained in ATCC-formulated F-12K medium supplemented with 10% heat-inactivated FCS (HyClone), 1% penicillin/streptomycin (Gibco), and 50 μM of 2-mercaptoethanol (Gibco). All cell cultures were grown at 37 °C in a 5% CO_2 atmosphere. Cells were passaged at ∼80% confluence, and all experiments were performed within five cell passages after thawing.

Isolation and In Vitro Activation of Splenic Murine B and T Cells. Single cell suspensions were prepared from the spleens of 6 to 8 week old female BALB/c mice through mechanical dissociation using a 70 μm cell strainer (BD Biosciences). The cells were recovered in ice-cold serum-free RPMI media, after which the sample was centrifuged, and the pellet resuspended in ACK buffer for 10 min to lyse any red blood cells present. The obtained splenocytes were then washed twice with PBS and finally recovered in 10% FCS RPMI. When lymphocyte activation was not required, the cells were placed in 10% FCS RPMI for 12 h before transfection. When lymphocyte activation was required, we cultured the total splenocytes in 10% FCS RPMI media supplemented with an anti-CD28 monoclonal antibody

https://doi.org/10.1021/acs.biomac.2c00469
Biomacromolecules XXXX, XXX, XXX−XXX

(mAb) at 0.5 μg/mL (BD Pharmingen, hamster anti-mouse NA/LE) and an anti-CD3 mAb at 0.05 μg/mL (BD Pharmingen, hamster anti-mouse NA/LE) for 24 h at 37 °C in a 5% CO_2 atmosphere. This resulted in direct stimulation of T cells with subsequent cytokine production and bystander activation of the B cells in culture. After this, the cells were transferred to a 96-well plate and prepared for transfection.

Isolation and In Vitro Activation of Human Peripheral Blood B and T Lymphocytes. Healthy donor PBMCs were obtained from the Stanford University Medical Center blood bank and isolated by density-gradient centrifugation using the Ficoll-Hypaque technique (Amersham Biosciences). B cells were then extracted using a positive selection method based on CD19-specific magnetic microbeads (Miltenyi Biotec). T cells were extracted using a negative selection method based on anti-CD43 magnetic microbeads (Miltenyi Biotec). All specimens were obtained with informed consent in accordance with the Declaration of Helsinki, and this study was approved by Stanford University's Administrative Panels on Human Subjects in Medical Research. Samples were collected from patients by peripheral blood leukapheresis and were cryopreserved. After isolation, T cells were resuspended in AIM V serum-free medium (Thermo Fisher) supplemented with recombinant human IL-2 at 3000 U/mL (Thermo Fisher), anti-CD3 mAb at 1 μg/mL (BD Pharmingen, mouse anti-human NA/LE), anti-CD28 mAb at 5 μg/mL (BD Pharmingen, mouse anti-human NA/LE) and 2-mercaptoethanol (55 μM, Gibco). Once isolated, B cells were resuspended in 10% FCS RPMI supplemented with recombinant human IL-4 at 20 ng/mL (Invitrogen) and anti-CD40 mAb at 1 μg/mL (BD Pharmingen, mouse anti-human NA/LE). Both B and T cells were cultured in their respective activation media for 24 h at 37 °C in a 5% CO_2 atmosphere, after which the cells were transferred to a 96-well plate and prepared for transfection.

Flow Cytometry. The following fluorochrome-conjugated rat anti-mouse mAbs were used for flow cytometry: B220-PerCP-Cy5.5, CD21/CD35-FITC, CD11b-BV605 IgD-BV786, CD3-BV786, CD49b-eFlour450, CD3-PE, S1P1-PE, CD8-PerCP-Cy5,5, CD4-FITC, CD3-APC, CD19-PE, CD11b-PerCPCy5.5, CD69-PE, and rat isotype controls for the listed fluorochromes and antibodies. The following fluorochrome-conjugated mouse anti-human antibodies were used for flow cytometry: APC-S1P1, PerCpCy5.5-CD8, PE-CD4, and mouse isotype controls for the listed fluorochromes and antibodies. An anti-CD16/32 rat anti-mouse unconjugated antibody was used to block Fc receptor binding sites and prevent non-specific staining. All the above antibodies were purchased from BD Biosciences, Invitrogen, or eBioscience, except for the mouse anti-human APC-S1P1 and the rat anti-mouse PE-S1P1 antibodies, which were purchased from R&D Systems. All surface marker staining was done for 20 min at room temperature. Cells were surface stained in wash buffer [PBS, 0.5% BSA (Sigma), and 0.01% sodium azide], either fixed in 2% paraformaldehyde or run fresh and analyzed by flow cytometry on a FACSCalibur or LSR-II System (BD Biosciences). Data were analyzed using Cytobank (Cytobank Inc.).

mRNA. EGFP-mRNA (5meC, ψ, L-6101), Fluc mRNA (5meC, ψ, L-6107), and Cy5-Fluc mRNA (5meC, ψ, L-7702) were purchased from TriLink BioTechnologies Inc.

General CART Formulation Methods. Deprotected CARTs were dissolved in dimethyl sulfoxide (DMSO) to prepare 2 or 5 mM solutions for in vitro or in vivo applications, respectively. These solutions are then filtered through a 0.20 μm nylon syringe filter (Millex-GN) and stored at −20 °C until use. In a sterile negative pressure biosafety cabinet, CARTs were formulated with mRNA at a 10:1 cation/anion charge ratio, assuming full protonation of the CART and full deprotonation of the oligonucleotides. Formulations were made by mixing the reagents for 20 s in acidic PBS (pH adjusted to 5.5 by addition of 0.1 mol/L HCl) in a total volume of 56−250 μL, followed by a brief spin in a tabletop centrifuge. In all experiments, mRNA was first mixed with PBS (pH 5.5) with subsequent addition of the CART (solution in DMSO). The resulting mRNA/CART formulation was then used immediately for in vitro or in vivo experiments.

CART In Vitro Transfection. For all in vitro transfection experiments, immediately before treatment, the cells were washed twice with PBS, resuspended in serum-free media (RPMI or F-12K in the case of CHO cells), and then seeded at a concentration of 1×10^5/well in a total volume of 40 μL. Then, CART formulations were prepared by adding 2.8 μg of mRNA (2.8 μL of a 1 mg/mL stock) to 49.3 μL of PBS (pH 5.5). To this, 3.92 μL of CART (from a 2 mmol/L stock in DMSO) was added and mixed for 20 s, obtaining a solution prepared in excess for 14 replicates. Then, 4 μL of the mixed mRNA/CART solution was immediately added to each well of a 96-well plate, obtaining either six or 12 replicates per condition and resulting in a final mRNA dose of 200 ng/well. This was incubated for 4 h at 37 °C (5% CO_2), after which the transfection reaction was quenched, and mRNA expression was analyzed based on the specific gene reporter assay employed as described below.

Free FTY720 Pre-treatment. When exposure to free FTY720 prior to transfection was required, cells were resuspended in 1.4 mL of 10% FCS RPMI media in FACS tubes at a cell density of 1×10^6/mL, and to this, FTY720 at either 5 nM or 5 ρM was added. The cells were then directly seeded in a 96-well plate at a density of 1×10^5 cells/well at a volume of 40 μL and then incubated at 37 °C (5% CO_2). After 30 min of incubation, the plate was centrifuged, the supernatant removed, and the pelleted cells resuspended in 40 μL/well of serum-free media, ready for treatment with different mRNA/CART polyplexes as described above.

EGFP mRNA Delivery and Expression into Cultured B and T Lymphocytes. B and T lymphocytes were prepared as above and incubated with the transfection mix for 4 h at 37 °C (5% CO_2), after which they were resuspended in 10% FCS RPMI media to quench the transfection reaction. At this point, the cells were either immediately analyzed (Figure S2B) or left in culture for an additional 24 h before analysis (Figure 3). To measure GFP expression, the plates were centrifuged, the supernatant removed, and the cells resuspended in PBS (150 μL/well). Then, for each experimental condition, cells from each of the 12 replicate wells were collected in two FACS tubes that were then analyzed in parallel through flow cytometry to quantify GFP expression (LSR-II System, BD Biosciences). Cells treated with EGFP mRNA only were used as negative controls.

Fluc mRNA Delivery and Expression into Jurkat, CHO, and K562 Cells. Jurkat, CHO, and K562 cells were prepared as above and incubated with the transfection mix for 4 h at 37 °C (5% CO_2), after which D-luciferin (Biosynth AG) at a concentration of 1 mM was added directly to the wells. The cells were then incubated at 37 °C for 10 min, and bioluminescence was measured immediately afterward through a single-mode microplate luminescence reader (SpectraMax L, Molecular Devices). Cells treated with Fluc mRNA only were used as negative controls. For each condition, bioluminescence was expressed as average relative luminescence units (RLUs) calculated as

$$[\text{Average luminescence for Fluc mRNA} - \text{CART treated wells } (n = 6 \text{ or } 12)] - [\text{Average luminescence for Fluc mRNA treated wells } (n = 6 \text{ or } 12)]$$

Error is expressed as ± SD.

CART In Vivo Transfection. For in vivo administration, CART formulations were prepared by adding 18.8 μg of mRNA (18.75 μL of a 1 mg/mL stock) to 205 μL of PBS (pH 5.5), and to this, 26.2 μL of CART (from a 2 mmol/L stock in DMSO) was added and mixed for 20 s. A total of 100 μL of this formulation was administered intravenously into the tail vein of each mouse, injecting two mice at a time per each treatment group and resulting in a final mRNA dose of 0.32 mg/kg (0.75 μg/mouse). CART formulations were injected immediately after mixing (within 20 s). The CART-mRNA formulations and the in vivo injections were performed under a negative pressure fume hood.

In Vivo Bioluminescence. 6 hours after administration of Fluc mRNA-CART complexes, mice were anesthetized with isoflurane gas, and D-luciferin was injected i.p. at a dose of 150 mg/kg. Fluc

https://doi.org/10.1021/acs.biomac.2c00469
Biomacromolecules XXXX, XXX, XXX−XXX

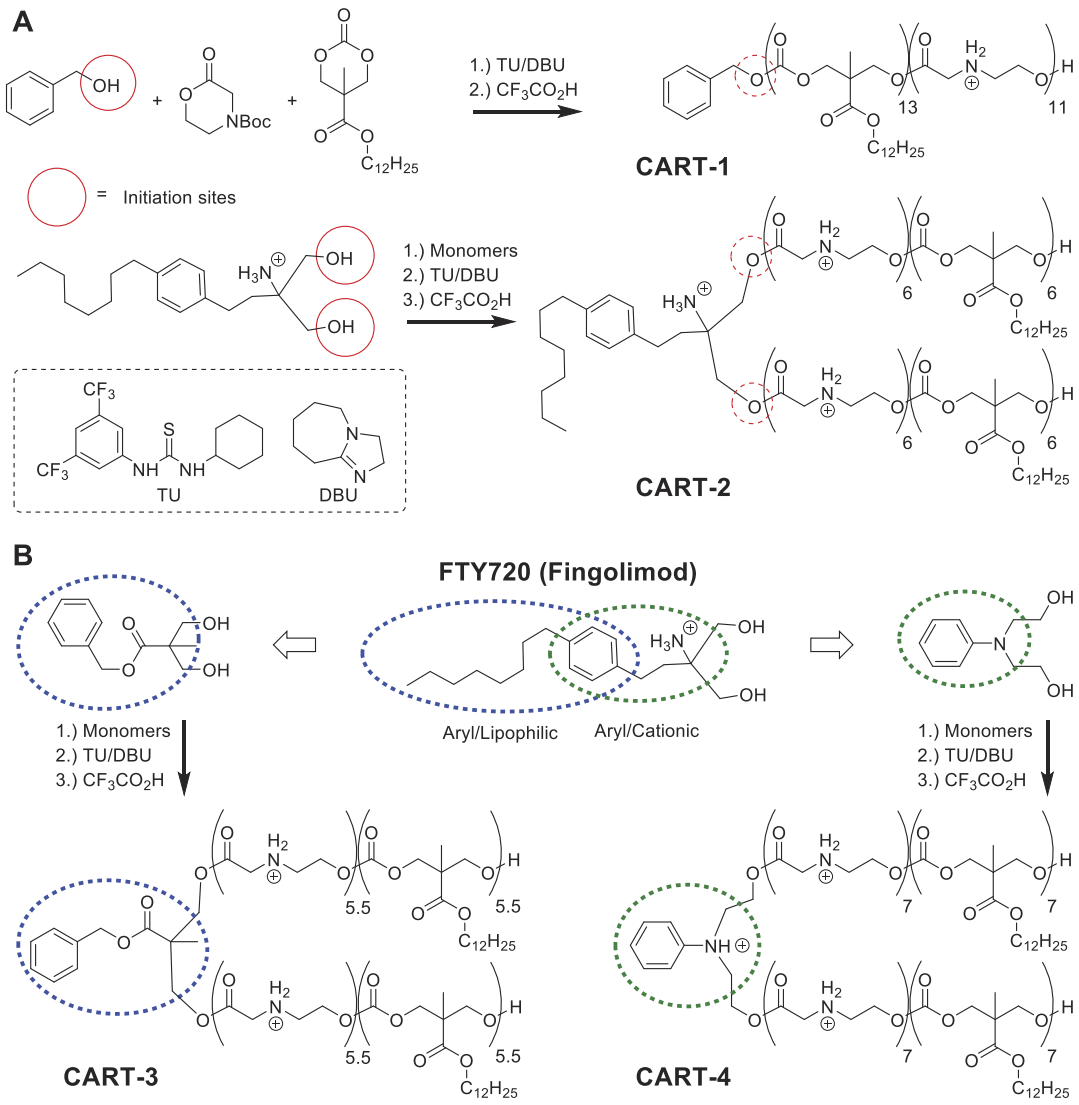

Figure 1. Synthesis and chemistry of CARTs. (A) Synthesis of **CART-2**: organocatalysts TU = 1-(3,5,bis(trifluoromethyl)phenyl)-3-cyclohexylthiourea, DBU = 1,8-diazabicyclo[5.4.0]undec-7-ene, (**CART-1** = benzyl, D13/A11; **CART-2** = FTY720, A12/D12). DP determined by ^{1}H NMR of the protected material. (B) Synthesis of **CART-3** and **CART-4**: aryl/lipophilic FTY720 analogue used for synthesis of **CART-3**: benzyl-2,2-bis(hydroxymethyl)propionate (B-DMPA); aryl/cationic FTY720 analogue used for synthesis of **CART-4**: *N*-phenyldiethanolamine (PhDEA). (**CART-3** = B-DMPA, A11/D11; **CART-4** = PhDEA, A14/D14). DP determined by ^{1}H NMR of the protected material.

expression was measured as whole-body bioluminescence 10 min after luciferin injection using an in vivo optical imaging system (IVIS 100; Xenogen Corp.). During image recording, mice were kept under anesthesia with isoflurane delivered via a nose cone, and their body temperature was maintained at 37 C°. Image analysis was performed with Living Image software (PerkinElmer).

In Vivo Cy5-mRNA Delivery to Murine Splenocytes. Formulations of Cy5-tagged Fluc mRNA and CARTs were prepared and administered intravenously (i.v.) as above. After 2 h, the mice were sacrificed, and the spleen was extracted and dissociated to a single cell suspension with a 70 μm cell strainer. Cells were recollected in serum-free RPMI, centrifuged, and resuspended in ACK buffer for 10 min to lyse the RBCs. After this, the cells were washed twice in PBS and then divided into three FACS tubes per treatment group. The cells were then stained with different lineage-specific antibodies and analyzed through flow cytometry to determine the % of Cy5$^+$ cells for each population.

Lymphocyte Depletion Assay. Blood was drawn from the submandibular vein of the mice immediately before and 24 h after treatment with Fluc mRNA-CART complexes prepared and administered as above. In both cases, approximately 1 mL of venous blood was collected per mouse into FACS tubes pre-filled with 500 μL of Ca^{2+}-EDTA. The blood samples were then centrifuged, the supernatant removed, and the pellet resuspended in ACK lysis buffer for 10 min. Then, the remaining PBMCs were washed twice with PBS and prepared for flow cytometry analysis.

Statistical Analysis. Prism software (GraphPad) was used to determine the statistical significance of differences between groups using the unpaired Student's *t*-test. *P* values < 0.05 were considered as statistically significant.

RESULTS AND DISCUSSION

Rationale for the Synthesis of FTY720-CART. The previously reported benzyl alcohol-initiated CART featuring dodecyl lipid side-chains (**CART-1**, Figure 1A) is a robust and effective gene delivery vehicle.[14,17] Here, we set out to design a CART delivery vehicle that incorporates an FTY720 ligand (fingolimod) inserted into the oligomeric backbone, intended to direct the CART preferentially to S1P1 overexpressing B cells and T cells and induce significant biological activity of

https://doi.org/10.1021/acs.biomac.2c00469
Biomacromolecules XXXX, XXX, XXX−XXX

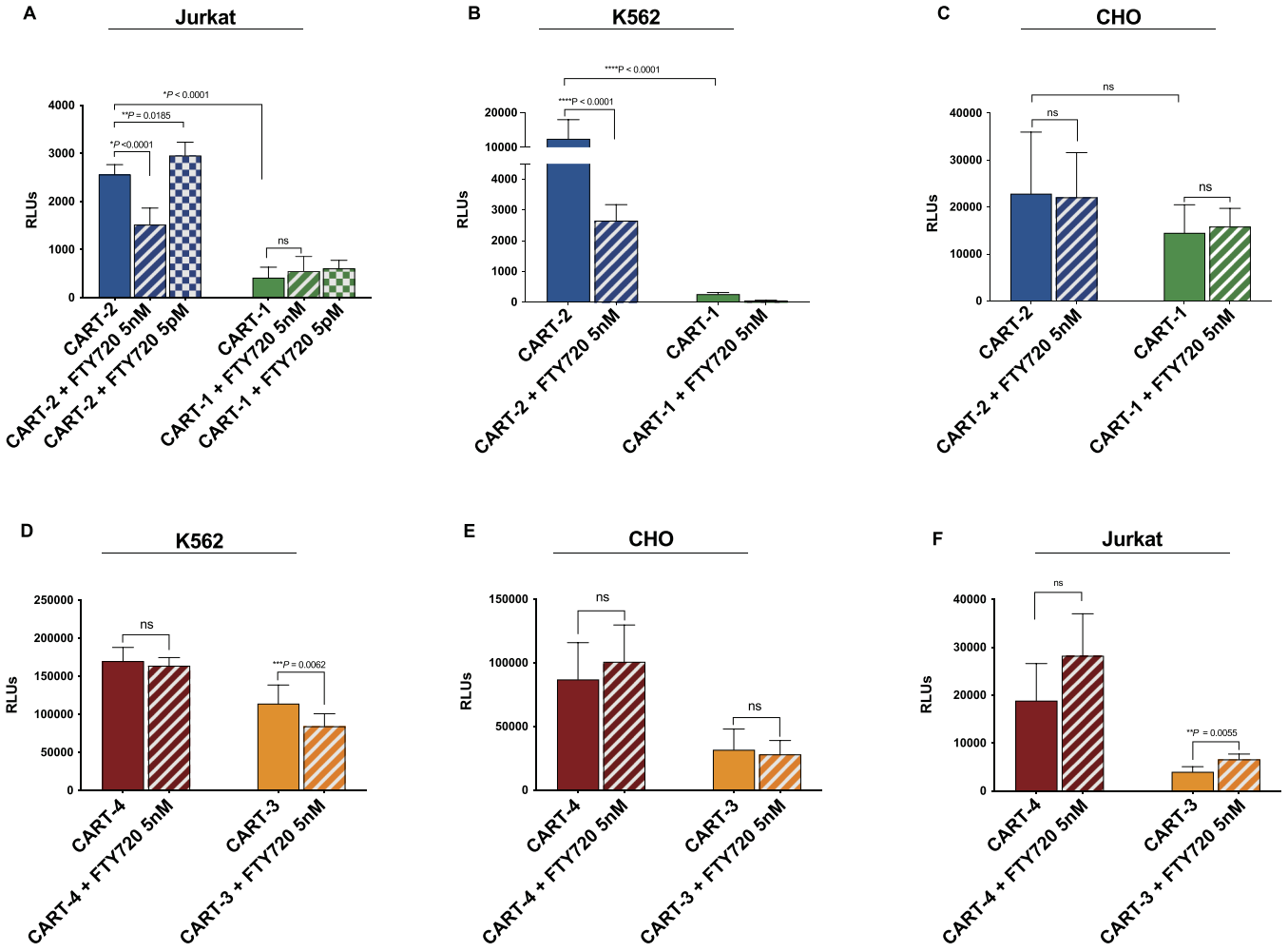

Figure 2. CART-2 outperforms **CART-1** in S1P1-expressing cells but not in S1P1-negative cells, and pre-exposure to FTY720 impairs **CART-2** transfection efficiency. Jurkat (A), K5620 (B), and CHO cells (C) were treated in vitro with Fluc mRNA complexed to either **CART-2** or **CART-1**, with and without pre-treatment with free FTY720 for 30 min at 5 nM or 5 pM. Luminescence was measured 4 h post transfection. Data show average RLUs for six replicates (Jurkat and CHO) or 12 replicates (K562). Cells treated with naked Fluc mRNA were used as negative controls, and their bioluminescence was subtracted from that of cells treated with the CART-mRNA complexes. Error bars show ± SD. K562 (D), CHO (E), and Jurkat cells (F) were treated in vitro with Fluc mRNA complexed to either the **CART-3** or **CART-4**, with and without 30 min pre-treatment with free FTY720 at 5 nM. Luminescence was measured at 4 h post transfection. Data show average RLUs for six replicates (CHO and K562) or 12 replicates (Jurkat). Cells treated with naked Fluc mRNA were used as negative controls, and their bioluminescence was subtracted from that of cells treated with the CART-mRNA complexes. Error bars show ± SD. Statistical significance was calculated using an unpaired Student's *t*-test (**P* < 0.001; ***P* < 0.05; ****P* < 0.01; ns, non-statistically significant).

those immune cells consistent with the known biological activity of fingolimod.

We synthesized biodegradable FTY720-containing CARTs by the ring-opening polymerization of *N*-boc morpholinone and MTC-dodecyl carbonate monomers initiated by an *N*-boc-protected FTY720 diol, which, because of the two alcohol initiation sites, generates a triblock structure (i.e., short oligomers from both ends of the FTY720 molecule) named **FTY720-CART** (**CART-2**, Figure 1A). The oligomerization was followed by global deprotection with TFA to reveal the fingolimod moiety as well as the ionizable α-amino ester groups of the amphiphilic oligomers.

From the end-group analysis by ^{1}H NMR of the protected material, the FTY720-initiated **CART-2** contains 12 total cationic monomers and 12 lipophilic monomers per initiator (**CART-2** = FTY720, A12/D12). In these studies, the previously reported diblock **CART-1** is included for comparison, which contains 13 lipophilic monomers and 11 cationic monomers per initiator (**CART-1** = benzyl, D13/A11).[12] Additionally, we synthesized triblock analogues of the FTY720-initiated **CART-2** to study specific effects of the FTY720 moiety (vide infra). One analogue is initiated with benzyl-2,2-bis(hydroxymethyl)propionate, B-DMPA (**CART-3**, Figure 1B) and contains 11 cationic monomers and 11 lipophilic monomers per initiator (data from protected material, **CART-3** = B-DMPA, A11/D11). The other analogue, initiated with *N*-phenyldiethanolamine, PhDEA (**CART-4**, Figure 1B), contains 14 cationic monomers and 14 lipophilic monomers per initiator (data from protected material, **CART-4** = PhDEA, A14/D14).

CART-2 Outperforms CART-1 Likely via an S1P1-Mediated Mechanism. We have previously demonstrated that CARTs effectively encapsulate and deliver mRNA to the cellular cytoplasm, both in vitro and in vivo, via a mechanism dependent on endocytosis and subsequent escape from the endosome.[12] We also showed that changes in the chemical

https://doi.org/10.1021/acs.biomac.2c00469
Biomacromolecules XXXX, XXX, XXX−XXX

structure of the CARTs can influence the types of cells transfected by the mRNA/CART polyplexes.[17]

To assess if a specific ligand−receptor interaction could preferentially increase mRNA delivery and expression in cells that harbor the surface receptor, we used a Fluc reporter gene assay to test if the novel **CART-2** more efficiently transfects cells that express S1P1. For these studies, we compared luciferase expression with either **CART-2** or its non-FTY720-conjugated analogue **CART-1** in cell lines expressing or lacking the S1P1 receptor (Figure 2). Specifically, the Jurkat and K562 cell lines were used as an S1P1-expressing cellular model,[24−26] and the CHO cell line was used as a model that naturally lacks expression for S1P1 (Figure S1). 4 h after treatment, mRNA expression was measured as relative bioluminescence of the cells treated with CART/mRNA complexes compared to cells treated with naked Fluc mRNA, which were used as negative controls. In Jurkat and K562 cells, **CART-2** achieved a sixfold and a 48-fold increase in Fluc expression, respectively, compared to **CART-1** (Figure 2A,B). In contrast, in CHO cells, there was no difference in bioluminescence between cells treated with **CART-1** and those treated with **CART-2**, suggesting that a non-specific mechanism might be responsible for mRNA delivery mediated by **CART-2** in S1P1-negative cells (Figure 2C). These data indicate that the FYT720-CART (**CART-2**) is more effective than **CART-1** for transfecting immortalized cells expressing S1P1.

To further test if the improved efficacy of **CART-2** in transfecting these S1P1-expressing cells is mediated by a specific interaction with the S1P1 receptor, we exposed cell cultures to free FTY720 for 30 min before treatment with different mRNA/CART complexes. This pre-treatment with free FTY720 did not reduce surface expression of S1P1 in any of the cellular models we employed (Figures S1 and S2C), but is expected to competitively occupy S1P1 binding sites. We observed that after exposure to free FTY720 at 5 nM (EC_{50}), there was a 40% reduction in Fluc expression in Jurkat cells treated with **CART-2** but no change in luminescence in those treated with **CART-1** (Figure 2A). When Jurkat cells were exposed to free FTY720 at a lower 5 ρM dose for 30 min, there was no reduction in bioluminescence after treatment with **CART-2**, suggesting a dose-dependent phenomenon. In K562 cells, pre-treatment with free FTY720 led to a significant 80% decrease in Fluc expression with **CART-2** (Figure 2B); for **CART-1**, the low levels of Fluc expression make it difficult to assess the effect of FTY720 pre-treatment (Figure 2B). In contrast, for the S1P1-negative CHO cells, pre-exposure to free FTY720 at 5 nM did not affect Fluc expression after treatment with either **CART-2** or **CART-1** (Figure 2C).

Similar results were observed in primary murine B lymphocytes isolated from the spleen of BALB/c mice (Figure S2). Animals were sacrificed, and the spleen was extracted and rendered into a single cell suspension. Cells were then cultured for 12 h before transfection with EGFP mRNA complexed to either **CART-2** or **CART-1**. After 4 h, the cells were stained for surface lineage markers and analyzed by flow cytometry to quantify EGFP expression in B cells (Figure S2A). In this case, after a 30 min pre-exposure to free FTY720 at 5 nM, we observed a 50% reduction in EGFP expression among cells treated with **CART-2** and a 30% increase in GFP expression in cells treated with **CART-1** (Figure S2B). Splenic murine B lymphocytes are known to express S1P1 in vivo, and we confirmed the retained expression of S1P1 ex vivo (Figure S2C). These observations are consistent with the hypothesis that the improved transfection ability of **CART-2** for S1P1-expressing cells is mediated by a specific interaction with S1P1. While in vivo phosphorylation of FTY720 is necessary for its pharmacological activity, closely related analogues do not require phosphorylation.[27,28] It is not clear if in vivo phosphorylation of the modified FTY720 in **CART-2** is required for uptake of **CART-2**/mRNA in S1P1-expressing cells.

Probing Structural Effects with Additional CART Constructs. In addition to the presence of an active targeting moiety, which appears to mediate a specific interaction with S1P1, the triblock structure of **CART-2** differs significantly from the linear diblock architecture of **CART-1**. This raises the important question of what physicochemical differences the resulting NPs may exhibit and to what extent these differences impact efficacy or may impart passive targeting effects. In exploring these questions, we synthesized **CART-3** and **CART-4** as structural analogues of **CART-2**. Both **CART-3** and **CART-4** exhibit a triblock structure analogous to **CART-2** but feature initiator moieties only partially resembling FTY720, which is intended to reduce affinity for S1P1. **CART-3** features an initiator (B-DMPA) mimicking the aryl/lipophilic motif of FTY720 but lacking an ionizable amine, while **CART-4** features an initiator (PhDEA) presenting an aryl/cationic motif but lacking a lipophilic domain. We observe that CART/mRNA NPs formed from all of these CARTs (1−4) exhibit a similar size (effective diameter from DLS 140−160 nm, Table S1) and ζ potential (+50 to +80 mV, Table S1). Similarly, all of these CARTs provide >95% encapsulation efficiency of mRNA when mixed at a 10:1 (positive/negative) charge ratio (Figure S3), and the resulting NPs show no cellular toxicity in a MTT viability assay (Figure S4).[17]

CART-3 and **CART-4** were investigated for in vitro Fluc transfection assays in Jurkat, K562, and CHO cells with and without pre-exposure to free FTY720 at 5 nM for 30 min. **CART-3** and **CART-4** transfect all three cell lines effectively. Indeed, in all three cell lines, the total luminescence observed for **CART-4** seemed to be higher than that observed for **CART-1** or **CART-2**. **CART-3** showed higher transfection in K562 cells than **CART-2** but similar transfection to **CART-2** in Jurkat and CHO cells. Interestingly, for both **CART-3** and **CART-4,** luciferase expression did not change in either K562 or CHO cells upon pre-exposure to free FTY720 (Figure 2D,E), and in Jurkat cells, we observed a measurable increase (∼50%) in Fluc expression after pre-exposure to free FTY720 (Figure 2F). Hence, pre-exposure to free FTY720 impairs the transfection efficiency of **CART-2** but not of **CART-3** and **CART-4**, and this is true only in S1P1-expressing cells.

These results support the hypothesis that **CART-2**, which features an FTY720 moiety, has an S1P1-specific interaction which is conducive to mRNA delivery and translation in S1P1-expressing cells. This provides an example of the conjugation of a pharmacologically validated small-molecule ligand to a polymeric gene delivery vehicle supporting specific and efficient cellular transfection. Peptide-targeting ligands and sugar-based compounds, including GalNac and galactose, have been investigated in gene delivery vectors such as LNPs.[20,29−32] However, the data also highlight the complicated interplay of factors that lead to successful cellular transfection, as **CART-3** and **CART-4,** also provide generically high levels of transfection.

CART-2 Transfects Primary Human and Murine Lymphocytes More Efficiently Than CART-1. B and T

https://doi.org/10.1021/acs.biomac.2c00469
Biomacromolecules XXXX, XXX, XXX−XXX

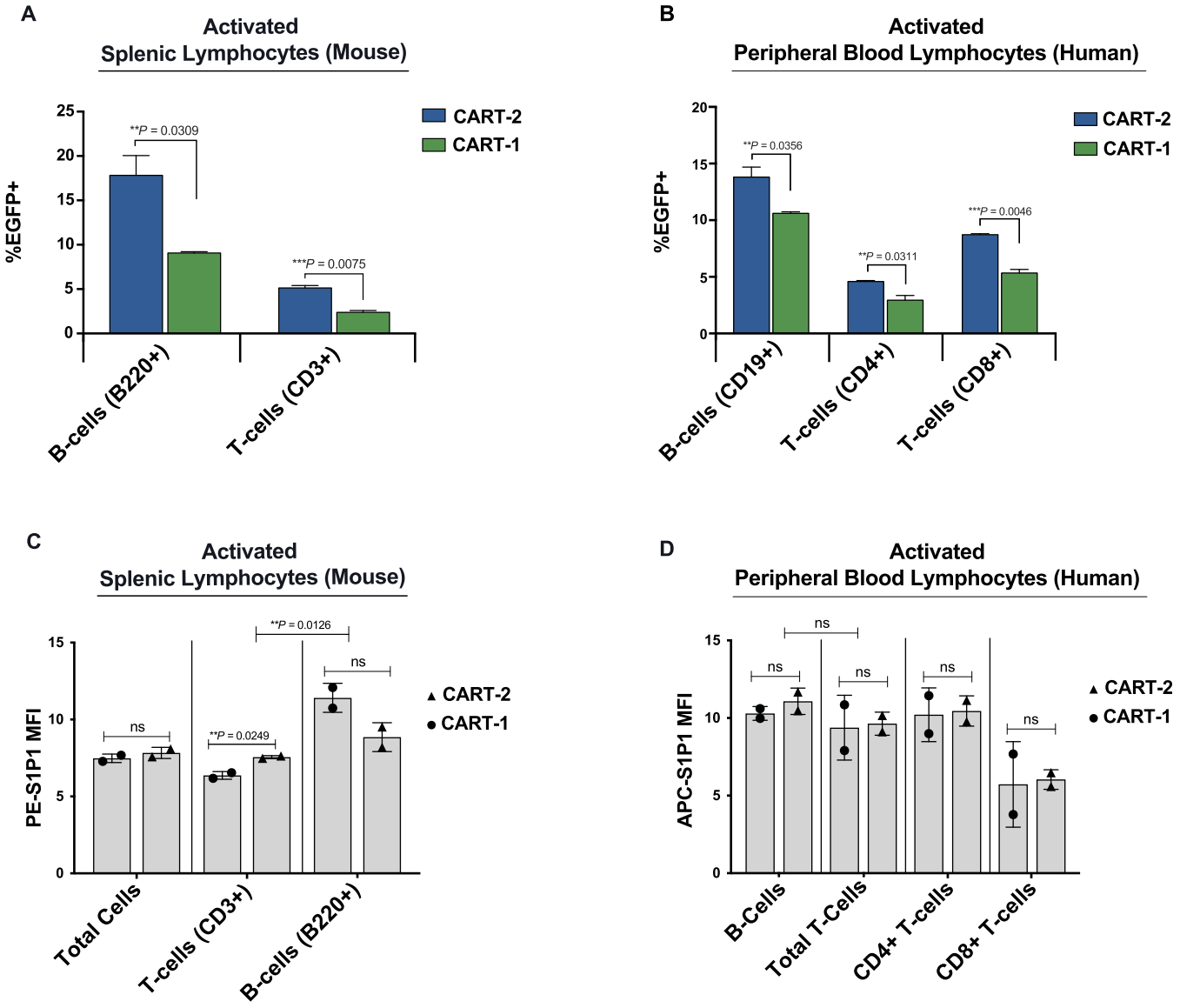

Figure 3. CART-2 transfects primary human and murine lymphocytes more efficiently than **CART-1.** Data show the average % of EGFP$^+$ cells in activated B and T murine splenic lymphocytes (A) and activated human B cells, CD4$^+$ T cells, and CD8$^+$ T cells from healthy donor PBMCs (B) treated with EGFP mRNA complexed to either **CART-1** (green) or **CART-2** (blue). EGFP expression was calculated through flow cytometry with two replicates per group. Error bars show ± SD. Statistical significance was calculated using an unpaired Student's *t*-test (*P < 0.001; **P < 0.05; ***P < 0.01; ns, non-statistically significant). (C) Data show the expression of the S1P1 receptor measured as the average median fluorescence intensity (MFI) of a S1P1-PE antibody on activated murine splenic T cells (CD3$^+$), B cells (B220$^+$), and total lymphocytes treated with either **CART-1** or **CART-2**. The MFI of cells treated with a PE-isotype antibody was subtracted from each group to control for background fluorescence. Error bars show ± SD (n = 2). Statistical significance was calculated using an unpaired Student's *t*-test (*P < 0.001; **P < 0.05; ***P < 0.01; ns, non-statistically significant). (D). Data show the expression of the S1P1 receptor measured as average MFI of an S1P1-APC antibody on activated human B cells, CD4$^+$ T cells, CD8$^+$ T cells, and total T cells isolated from healthy donor PBMCs treated with either **CART-1** or **CART-2**. The MFI of cells treated with an APC-isotype antibody was subtracted from each group to control background fluorescence. Error bars show ± SD (n = 2). Statistical significance was calculated using an unpaired Student's *t*-test (*P < 0.001; **P < 0.05; ***P < 0.01; ns, non-statistically significant).

lymphocytes use S1P receptors to sense the gradient of S1P that is naturally more concentrated in the blood compared to secondary lymphoid organs. S1P acts as a chemoattractant for B and T cells, mediating their egress from the spleen and lymph nodes (LNs) to the bloodstream. Also, S1P1 is usually upregulated after activation of lymphocytes to favor their exit from secondary lymphoid organs and accumulation in areas of active immune response (Figure S5).[33] Given the key role that S1P1 plays in the biology of B and T cells, we asked if **CART-2** could more efficiently transfect primary lymphocytes compared to its non-FTY720-initiated analogue, **CART-1**. To address this question, we used primary-activated murine and human B and T lymphocytes (Figure 3) since transfection efficiency is low in resting lymphocytes in vitro (Figure S2).

First, we extracted primary B and T lymphocytes from a murine spleen and co-cultured them in vitro for 24 h with anti-CD3 and anti-CD28 antibodies added to the growth medium to obtain direct activation of T cells and bystander activation of B cells.[34] Cells were then treated with EGFP mRNA complexed to either **CART-1** or **CART-2** (Figure 3A). After 4 h, the cell medium was replaced with fresh serum-containing medium, and the cells were then cultured for an additional 24

https://doi.org/10.1021/acs.biomac.2c00469
Biomacromolecules XXXX, XXX, XXX−XXX

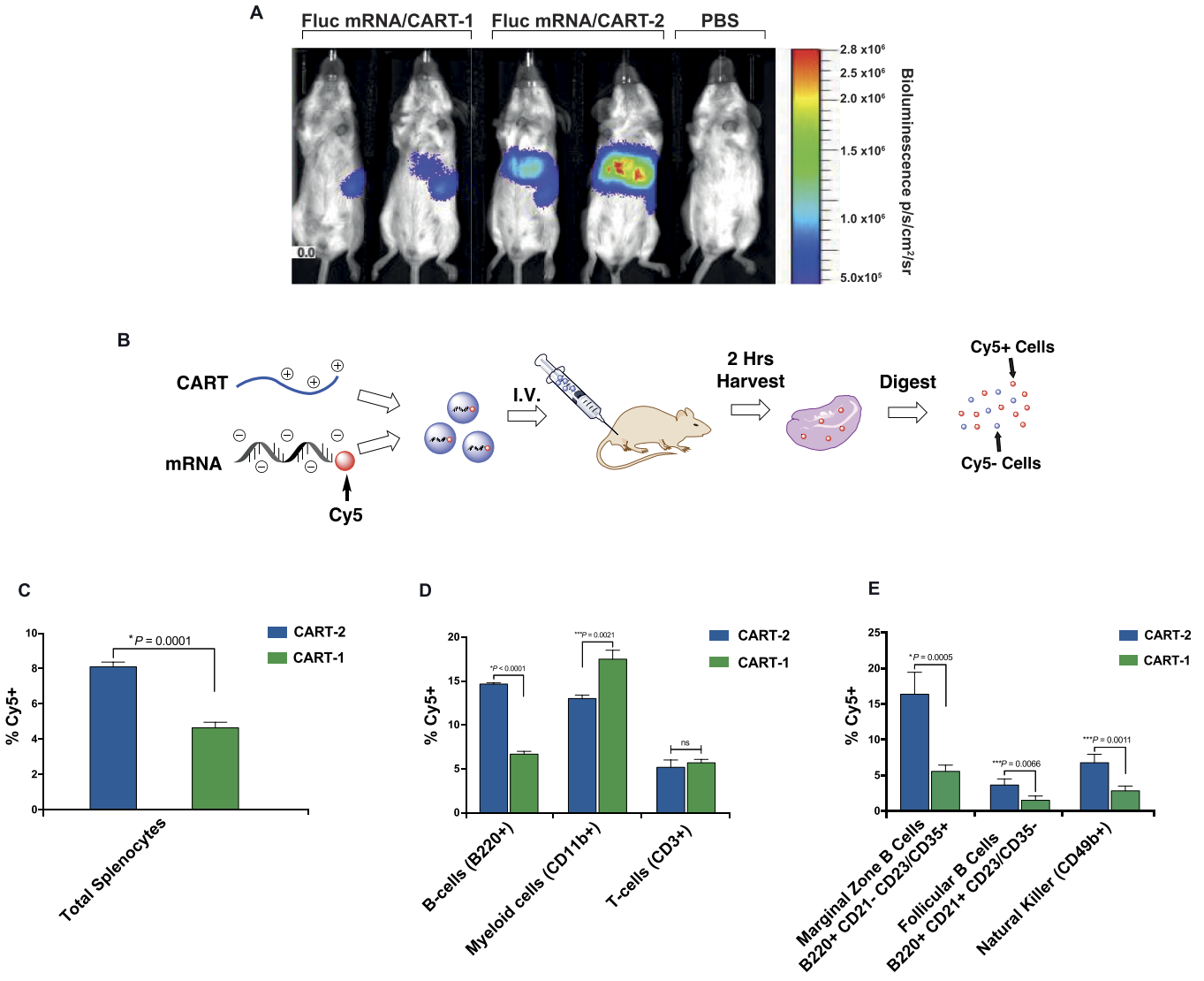

Figure 4. CART-2 shows increased mRNA delivery to splenic MZ B cells and NK cells in vivo compared to **CART-1**. (A) **CART-2** and **CART-1** each complexed to mRNA coding for the firefly luciferase reporter gene (Fluc) were administered i.v. to BALB/c mice. Whole-body bioluminescence was measured 6 h later and is represented here. (B) **CART-2** or **CART-1** complexed to Cy5-labeled Fluc mRNA was administered i.v. to BALB/c mice with two animals per group. After 2 h, the mice were sacrificed, and the spleens were extracted for mechanical isolation of the total splenocytes. The cells were then stained for flow cytometry analysis. (C) Data show average % of $Cy5^+$ cells in total splenocytes of animals treated with **CART-1** (green) and **CART-2** (blue). Error bars show ± SD for three staining replicates. (D) Data show average % of $Cy5^+$ cells in splenic B cells, myeloid cells, and T cells for animals treated with **CART-1** (green) and **CART-2** (blue). Error bars show ± SD for three staining replicates. (E) Data show average % of $Cy5^+$ cells in the splenic marginal zone B cells, follicular B cells, and NK cells for animals treated with **CART-1** (green) and **CART-2** (blue). Error bars show ± SD for four staining replicates. Statistical significance was calculated using an unpaired Student's *t*-test (*$P < 0.001$; **$P < 0.05$; ***$P < 0.01$; ns, non-statistically significant).

h, after which they were analyzed through flow cytometry to determine EGFP expression in both T cells ($CD3^+$) and B cells ($B220^+$, Figure S6). In this case, we observed, respectively, a 97% and an 89% increase in EGFP expression in B and T lymphocytes after treatment with **CART-2** compared to **CART-1**. Cell activation was confirmed by measuring CD69 expression on both B and T cells (Figure S7).

Comparable results were observed in primary human lymphocytes. In this case, peripheral blood mononuclear cells (PBMCs) from healthy donors were thawed, and B and T lymphocytes were isolated with lineage-specific magnetic microbeads. After isolation, B cells were cultured for 12 h in the presence of human IL-4 (20 ng/mL) and anti-CD40 (1 μg/mL) to obtain direct B cell activation.[35] Similarly, after isolation, T cells were cultured for 12 h and activated by the addition to the culture medium of anti-CD3 (1 μg/mL), anti-CD28 (5 μg/mL), and IL-2 (3000 UI/mL). T- and B-lymphocytes were then treated in parallel with EGFP mRNA complexed to either **CART-2** or **CART-1**. After 4 h, the cell medium was replaced with fresh serum-containing medium, and the cells were then cultured for an additional 24 h before EGFP expression was measured through flow cytometry (Figures 3B, S8).

In activated human B lymphocytes, EGFP expression was 38% higher in cells treated with **CART-2** compared to that in **CART-1**. Also, treatment of activated human T cells with **CART-2** showed a 55 and 64% increase in EGFP expression, respectively, in the $CD4^+$ and $CD8^+$ sub-populations,

https://doi.org/10.1021/acs.biomac.2c00469
Biomacromolecules XXXX, XXX, XXX−XXX

compared to **CART-1**. The expression of S1P1 was confirmed through flow cytometry on total activated murine splenic lymphocytes with higher levels on B cells compared to T cells, similar levels on B cells treated with **CART-1** compared to **CART-2,** and higher levels on T cells treated with **CART-2** compared to **CART-1** (Figure 3C). We also confirmed S1P1 expression on activated human B cells and activated human T cells with no difference in S1P1 levels between the two populations, as well as between cells treated with **CART-2** or **CART-1** in either B cells, total T cells, $CD4^+$ T cells, or $CD8^+$ T cells (Figure 3D).

Thus, our results show that **CART-2** can more efficiently transfect primary B and T lymphocytes in vitro compared to its non-FTY720-initiated analogue, **CART-1**. S1P1 expression levels did not seem to correlate with the transfection efficiency of either **CART-1** or **CART-2**. Indeed, both in human and murine B and T lymphocytes, **CART-2** outperformed **CART-1,** and mRNA expression was higher in B cells compared to T cells, even though S1P1 levels were similar between human B and T cells but slightly higher in murine B cells compared to murine T cells. Hence, the presence of S1P1 on the cell surface, rather than its expression level, seemed to correlate with the observed superiority of **CART-2** compared to **CART-1**.

This is particularly significant from a therapeutic standpoint since there is a growing demand for better technologies to transfect lymphocytes in vitro as it is needed, for example, in the development of adoptive T cell cancer immunotherapy strategies.[36]

CART-2 Efficiently Delivers mRNA to Splenic Marginal Zone B Cells and NK Cells In Vivo. To assess if the presence of FTY720 in the structure of the CART would change the organs and cells targeted in vivo by **CART-2** compared to its non-FTY720 analogue **CART-1**, we complexed mRNA coding for Fluc to either **CART-2** or **CART-1**. We then injected the resulting mRNA/CART complexes i.v. to BALB/c mice and measured whole-body bioluminescence (BLI) 6 h after the injections (Figure 4A). In animals treated with **CART-2,** bioluminescence emanated from both the spleen and the liver, while in animals treated with **CART-1,** bioluminescence was predominantly localized to the spleen, with a trend for higher total bioluminescence in mice treated with **CART-2** compared to **CART-1**.

Given the key role that the spleen plays in regulating systemic immune responses,[37] we then asked if there was a difference in the cells targeted within the spleen by the mRNA/**CART-2** compared to the mRNA/**CART-1** complexes. To address this question, we used Fluc mRNA conjugated to the cyanine 5 fluorophore (Cy5-mRNA). The Cy5-mRNA was mixed with either **CART-2** or **CART-1,** and the resulting mixtures were administered i.v. to BALB/c mice (Figure 4B). The animals were sacrificed 2 h later, and the spleens were extracted to obtain a single cell suspension that was then analyzed through flow cytometry to determine Cy5-mRNA delivery to specific cellular sub-populations. First, we observed that the total percentage of $Cy5^+$ cells in the spleen was 80% higher in animals treated with **CART-2** compared to **CART-1** (Figures 4C, S10A). We then measured Cy5-mRNA uptake in splenic B cells ($CD19^+$), T cells ($CD3^+$), and myeloid cells ($CD11b^+$) separately (Figures 4D and S9B−D). In this case, we found no difference in mRNA delivery to T cells between mice treated with **CART-2** and those treated with **CART-1**, while there was a 118% increase in mRNA delivery to B cells in animals treated with **CART-2** compared to those treated with **CART-1**, and a 34% increase in delivery of mRNA to myeloid cells in mice that received **CART-1** compared to **CART-2**.

In the murine spleen and similarly, in the human spleen, there are two main B cell populations, the marginal zone B cells (MZ B) and the follicular B cells (FO B), that differ significantly in terms of S1P1 expression and responsiveness to S1P in vivo.[38,39] Specifically, MZ B cells are specialized antigen-presenting cells (APCs) that constantly collect and transport antigens from the bloodstream to the follicles where they are processed and presented to FO B cells to elicit humoral immune responses. During this perpetual shuttling between the follicles and the marginal zone, the MZ B cells follow the gradient of S1P via the S1P receptors 1 and 3 (S1P1 and S1P3) to migrate from the follicle back to the marginal zone.[40] FO B cells instead show lower expression of S1P1 and lower responsiveness to S1P compared to the MZ B cells.[38] Given the higher S1P1 expression in splenic MZ B compared to FO B cells, we asked if there was a difference in the proportion of MZ B cells and FO B cells targeted by **CART-2** and **CART-1**. To answer this question, in a separate experiment, we again formulated Cy5-mRNA to either **CART-2** or **CART-1** and administered the complexes i.v. to BALB/c mice (Figures 4E and S10). Animals were sacrificed 2 h later to analyze mRNA delivery to splenic MZ B cells and FO B cells through flow cytometry. MZ B cells were defined as $B220^+$ $CD23^-$ $CD21/CD35^+$ cells, while FO-B cells were defined as $B220^+$ $CD23^+$ $CD21/CD35^-$.[41] In animals treated with **CART-2,** the average percentage of $Cy5^+$ MZ B cells and $Cy5^+$ FO B cells was, respectively, 192 and 140% higher compared to animals treated with **CART-1**. Also, the percentage of $Cy5^+$ MZ B cells was 355% higher than that of FO B cells in animals treated with **CART-2**, while in animals treated with **CART-1,** the percentage of Cy-5^+ MZ B cells was only 270% higher than what was seen in FO B cells. Thus, **CART-2** transfected both splenic B cell populations more effectively than **CART-1**, and the improvement was more pronounced in the MZ B cell population, which is the population that expresses more S1P1. In the same experiment, we also looked at mRNA delivery to splenic natural killer (NK) cells ($CD49b^+$) that are known to express S1P5, to which FTY720 has a lower but still significant affinity.[42,43] In this case, we found a 142% increase in the percentage of splenic $Cy5^+$ $CD49b^+$ cells after treatment with **CART-2** compared to **CART-1**.[44]

Overall, these results suggest that FTY720-conjugated **CART-2** provides increased mRNA delivery to the liver and spleen of living animals after intravenous administration of the mRNA/CART complex compared to **CART-1**. Also, within the spleen, **CART-2** more efficiently delivered mRNA to splenic MZ B cells and NK cells compared to **CART-1**, which could be particularly important from a therapeutic standpoint. MZ B cells play a significant role as APCs in starting both humoral and cellular immune responses against bloodborne antigens.[36,42] This subset of B lymphocytes is also involved in the generation of immune tolerance, and dysregulation of MZ B cells has been implicated in the pathophysiology of autoimmune diseases like systemic lupus erythematosus.[45,46] There is growing evidence that MZ B cells could be targeted for treatment of cancer and infectious diseases.[47] For example, a previous study has shown that it is possible to elicit a systemic anti-tumor T cellular response in mice after

https://doi.org/10.1021/acs.biomac.2c00469
Biomacromolecules XXXX, XXX, XXX−XXX

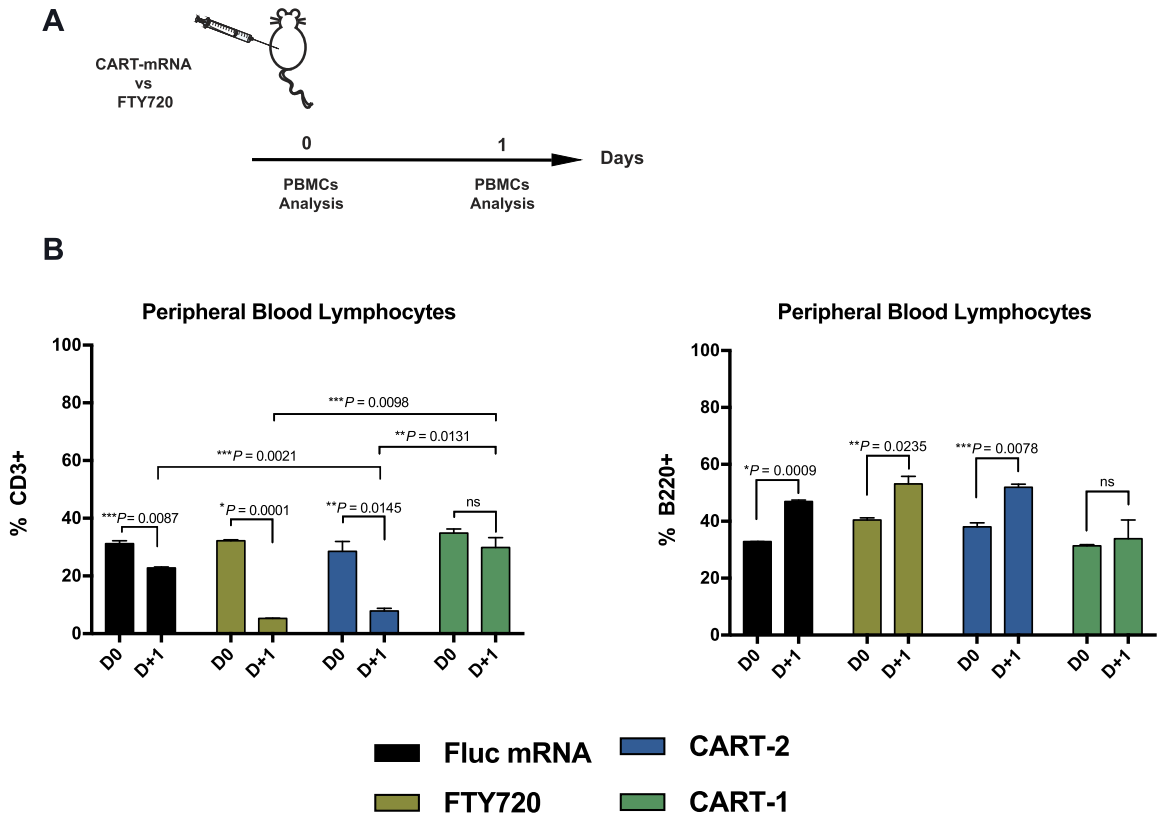

Figure 5. CART-2 induces lymphopenia similar to free FTY720. (A). BALB/c mice were treated with either **CART-1** or **CART-2** formulated with Fluc mRNA. Mice treated with free FTY720 or naked Fluc mRNA were used as positive and negative controls, respectively. All treatments were given i.v. Before treatment, the blood was drawn from each mouse to calculate the baseline percentage of circulating T cells ($CD3^+$) and B cells ($B220^+$) among the total lymphocytes. One day after treatment, mice were bled again to check for depletion of B and T cells from the peripheral blood. (B). Trend over time of the average % of $CD3^+$ (left) and $B220^+$ (right) peripheral blood lymphocytes in the different treatment groups. Error bars show ± SD for two replicates per group. Statistical significance was calculated using an unpaired Student's *t*-test (*$P < 0.001$; **$P < 0.05$; ***$P < 0.01$; ns, non-statistically significant).

intravenous administration of NPs that selectively deliver tumor-associated antigens to splenic MZ B cells.[48] **CART-2** was able to effectively deliver mRNA to 7% of the splenic NK cell population after intravenous administration in mice. The observation of mRNA uptake in NK cells is intriguing as these difficult-to-transfect class of lymphocytes play a significant role in cancer immune surveillance and offer a new target for cancer immunotherapy.[49] We have recently shown that CARTs can efficiently transfect primary human NK cells in vitro to generate NK-chimeric antigen receptor cells.[50] This property of **CART-2** could be exploited to manipulate NK cells in vivo to generate potent systemic anti-tumor immune responses.

CART-2 Induces Peripheral T Cell Depletion Similarly to Free FTY720. One of the potential benefits of functionalizing an mRNA delivery vehicle with a small molecule is to exploit the biological properties of the small molecule for therapeutic purposes. FTY720 exerts its immunosuppressive effects by segregating T and B cells in secondary lymphoid organs, thus interfering with their migration to sites of active immune response.[51,52] We thus asked if **CART-2**, featuring an FTY720 moiety, could induce lymphopenia in animals. To answer this question, we treated BALB/c mice with either free FTY720, naked Fluc mRNA, or Fluc mRNA complexed to **CART-1** or **CART-2**, all administered i.v. The mice that received free FTY720 were treated with 12.9 μg of FTY720 to match the amount of molecular FTY720 present in each dose of Fluc mRNA/**CART-2**. Also, the mice that received naked Fluc mRNA were administered the same amount of mRNA present in each mRNA/CART complex (7.5 μg/mouse). Before treatment, mice were bled to measure the baseline levels of circulating T cells ($CD3^+$) and B cells ($B220^+$) calculated through flow cytometry as a percentage of the total peripheral blood lymphocytes (Figure S12). The mice were then bled 24 h after treatment, and the levels of peripheral T and B lymphocytes were measured again (Figure 5). As expected, in mice treated with free FTY720, we observed an 84% reduction in the percentage of circulating T cells 1 day after treatment. Similar results were observed in mice treated with Fluc mRNA/**CART-2**, where there was a 72% reduction in circulating T cells. Instead, there was no reduction in the proportion of circulating T lymphocytes in animals that received Fluc mRNA/**CART-1**, while in mice treated with only Fluc mRNA, we observed a 27% decrease in the percentage of circulating T cells. This small decrease in the proportion of circulating lymphocytes observed with naked mRNA administration could be an artifact caused by the innate activating properties of naked mRNA.[53−55] Looking at peripheral B cells, in animals treated with either free FTY720, naked Fluc mRNA, or Fluc mRNA/**CART-2**, we observed an increase in the percentage of circulating B cells 24 h after treatment, possibly secondary to the concomitant reduction in circulating T cells. In contrast, in animals that received Fluc mRNA/**CART-1**,

https://doi.org/10.1021/acs.biomac.2c00469
Biomacromolecules XXXX, XXX, XXX−XXX

there was no change in the percentage of circulating B cells after treatment.

Hence, animals treated with **CART-2** showed almost complete peripheral T cell depletion, similar to those that received free FTY720. However, neither free FTY720 nor **CART-2** caused a depletion of circulating B cells. One explanation for the lack of effect on circulating B cells is that the dose of FTY720 used in our experiments was 12.9 μg/mouse (approximately 0.7 mg/kg), while previous data showed B cell depletion at a FTY720 dose of 2.5 mg/kg per mouse.[56] Also, in prior studies, B cell depletion was observed with daily oral administration to mice over a period of 21 days, while in our experiments, we administered a single dose of FTY720 intravenously and assessed B cell depletion 24 h later.[57]

Overall, these results suggest that the FTY720 moiety retains, at least in part, its biological activity when present in the structure of **CART-2,** or that free FTY720 is released from **CART-2** over time due to the known charge-altering self-immolation behavior of CARTs.[12] This observation suggests therapeutic opportunities for these and other related CART constructs. For example, **CART-2** could potentially be used to develop a combination small-molecule mRNA-based therapy not only for multiple sclerosis but also for general autoimmune disorders.

CONCLUSIONS

The versatile chemistry of the CART delivery platform was leveraged to conjugate a single small-molecule drug, FTY720, to the core backbone of the CART to generate a triblock co-oligomer. We specifically chose to use FTY720 given its known interactions with the S1P receptor 1, which is present on T and B lymphocytes in secondary lymphoid organs. We further leveraged the CART platform by generating CARTs initiated with FTY720-mimics (**CART-3** and **CART-4**) to better elucidate the specific effects of the FTY720-initiated CART (**CART-2**). Our main goal was to create an mRNA delivery vehicle that was able to deliver mRNA more efficiently and more selectively to lymphocytes for therapeutic purposes, both in vitro and in vivo.

Here, we showed that the novel **CART-2** is superior to its non-FTY720-initiated analogue, **CART-1,** in transfecting cells that express S1P1, while the two CARTs are equivalent in cells that lack expression of S1P1. **CART-2** was also particularly effective in transfecting activated human and murine B and T cells in vitro, which can be significant from a clinical and therapeutic standpoint. Also, transfection with **CART-2** was impaired by pre-exposure of target cells to free FTY720, indicative of an S1P1-mediated mechanism for mRNA delivery with **CART-2**. Thus, we provide an example of the conjugation of a pharmacologically validated small-molecule ligand to a polymeric gene delivery vehicle supporting specific and efficient cellular transfection—an approach that complements the similar application of peptide-targeting ligands and sugar-based compounds, including GalNac and galactose, in gene delivery vectors such as LNPs.[20,29−32]

Upon intravenous administration, we observed uptake of mRNA in splenocytes, B cells, marginal zone B cells, and NK cells in the spleen, with higher mRNA delivery observed for **CART-2** than for **CART-1**. These properties of **CART-2** are particularly appealing for potential applications in cancer immunotherapy as well as vaccine development and treatment of autoimmune diseases.

Lastly, we found that **CART-2** causes depletion of T lymphocytes from the peripheral blood similarly to free FTY720, suggesting that FTY720-conjugated CARTs elicit responses mediated both by the mRNA and the small molecule incorporated into its structure. This finding further increases the therapeutic potential of the CARTs, with the possibility of achieving synergistic effects between the mRNA cargo and the small molecule conjugated to the CART polymer.

ASSOCIATED CONTENT

Supporting Information

The Supporting Information is available free of charge at https://pubs.acs.org/doi/10.1021/acs.biomac.2c00469.

S1P1 expression on CHO, Jurkat, and K562 cells; primary murine B lymphocytes; CD69 expression on in vitro-activated murine B and T cells; S1P1 expression on in vitro-activated murine B and T cells; gating strategy for flow cytometry data; size and ζ potential measurements of **CART-1**, **CART-2**, **CART-3,** and **CART-4**; mRNA encapsulation efficiency for **CART-2**, **CART-3,** and **CART-4**; MTT viability assay of **CART-2**, **CART-3,** and **CART-4** on HeLA cells; additional experimental details; and ^{1}H NMR spectra for all CARTs (PDF)

AUTHOR INFORMATION

Corresponding Author

Ronald Levy − *Stanford Cancer Institute, Division of Oncology, Department of Medicine, Stanford University, Stanford, California 94305, United States*; Email: levy@stanford.edu

Authors

Stefano Testa − *Stanford Cancer Institute, Division of Oncology, Department of Medicine, Stanford University, Stanford, California 94305, United States*; orcid.org/0000-0001-5632-5021

Ole A. W. Haabeth − *Stanford Cancer Institute, Division of Oncology, Department of Medicine, Stanford University, Stanford, California 94305, United States*

Timothy R. Blake − *Stanford Cancer Institute, Division of Oncology, Department of Medicine, Stanford University, Stanford, California 94305, United States; Department of Chemistry, Stanford University, Stanford, California 94305, United States*

Trevor J. Del Castillo − *Department of Chemistry, Stanford University, Stanford, California 94305, United States*; orcid.org/0000-0001-5120-1935

Debra K. Czerwinski − *Stanford Cancer Institute, Division of Oncology, Department of Medicine, Stanford University, Stanford, California 94305, United States*

Ranjani Rajapaksa − *Stanford Cancer Institute, Division of Oncology, Department of Medicine, Stanford University, Stanford, California 94305, United States*

Paul A. Wender − *Department of Chemistry and Department of Chemical and Systems Biology, Stanford University, Stanford, California 94305, United States*; orcid.org/0000-0001-6319-2829

Robert M. Waymouth − *Department of Chemistry, Stanford University, Stanford, California 94305, United States*; orcid.org/0000-0001-9862-9509

Complete contact information is available at: https://pubs.acs.org/10.1021/acs.biomac.2c00469

https://doi.org/10.1021/acs.biomac.2c00469
Biomacromolecules XXXX, XXX, XXX−XXX

Author Contributions

O.A.W.H. and T.R.B. contributed equally to this work. The article was written through contributions of all authors. All authors have given approval to the final version of the article.

Notes

The authors declare the following competing financial interest(s): Ronald Levy serves on the Scientific Advisory Boards of Quadriga, BeiGene, GigaGen, Teneobio, Nurix, Dragonfly, Apexigen, Viracta, Spotlight, Immunocore, Walking Fish, Kira, Abintus Bio, Khloris, Virsti, BiolineRx. The other authors have no conflicts of interest to declare.

■ ACKNOWLEDGMENTS

This work was supported by an American-Italian Cancer Foundation Post-Doctoral Research Fellowship (to S.T.); by grants 5R01CA245533-03 (R.M.W., P.A.W., and R.L.), R35 CA19735301A (to R.L.), and CA031845 to (P.A.W.) from the National Institutes of Health and by grants CHE-848280 (P.A.W.) and CHE-2002933 (R.M.W.) from the National Science Foundation (organocatalytic polymerization). Part of this work was performed at the Stanford Nano Shared Facilities (SNSF) supported by the National Science Foundation under award ECCS-2026822.

■ REFERENCES

(1) Paunovska, K.; Loughrey, D.; Dahlman, J. E. Drug delivery systems for RNA therapeutics. *Nat. Rev. Genet.* **2022**, *23*, 265−280.

(2) Batty, C. J.; Heise, M. T.; Bachelder, E. M.; Ainslie, K. M. Vaccine formulations in clinical development for the prevention of severe acute respiratory syndrome coronavirus 2 infection. *Adv. Drug Delivery Rev.* **2021**, *169*, 168−189.

(3) Meo, S. A.; Bukhari, I. A.; Akram, J.; Meo, A. S.; Klonoff, D. C. COVID-19 vaccines: comparison of biological, pharmacological characteristics and adverse effects of Pfizer/BioNTech and Moderna Vaccines. *Eur. Rev. Med. Pharmacol. Sci.* **2021**, *25*, 1663−1669.

(4) Baden, L. R.; El Sahly, H. M.; Essink, B.; Kotloff, K.; Frey, S.; Novak, R.; Diemert, D.; Spector, S. A.; Rouphael, N.; Creech, C. B.; McGettigan, J.; Khetan, S.; Segall, N.; Solis, J.; Brosz, A.; Fierro, C.; Schwartz, H.; Neuzil, K.; Corey, L.; Gilbert, P.; Janes, H.; Follmann, D.; Marovich, M.; Mascola, J.; Polakowski, L.; Ledgerwood, J.; Graham, B. S.; Bennett, H.; Pajon, R.; Knightly, C.; Leav, B.; Deng, W.; Zhou, H.; Han, S.; Ivarsson, M.; Miller, J.; Zaks, T.; Group, C. S. Efficacy and Safety of the mRNA-1273 SARS-CoV-2 Vaccine. *N. Engl. J. Med.* **2021**, *384*, 403−416.

(5) Walsh, E. E.; Frenck, R. W.; Falsey, A. R.; Kitchin, N.; Absalon, J.; Gurtman, A.; Lockhart, S.; Neuzil, K.; Mulligan, M. J.; Bailey, R.; Swanson, K. A.; Li, P.; Koury, K.; Kalina, W.; Cooper, D.; Fontes-Garfias, C.; Shi, P.-Y.; Türeci, Ö.; Tompkins, K. R.; Lyke, K. E.; Raabe, V.; Dormitzer, P. R.; Jansen, K. U.; Şahin, U.; Gruber, W. C. Safety and Immunogenicity of Two RNA-Based Covid-19 Vaccine Candidates. *N. Engl. J. Med.* **2020**, *383*, 2439−2450.

(6) Guevara, M. L.; Persano, F.; Persano, S. Advances in Lipid Nanoparticles for mRNA-Based Cancer Immunotherapy. *Front. Chem.* **2020**, *8*, 589959.

(7) Mi, P.; Cabral, H.; Kataoka, K. Ligand-Installed Nanocarriers toward Precision Therapy. *Adv. Mater.* **2020**, *32*, 1902604.

(8) Yoo, J.; Park, C.; Yi, G.; Lee, D.; Koo, H. Active Targeting Strategies Using Biological Ligands for Nanoparticle Drug Delivery Systems. *Cancers* **2019**, *11*, 640.

(9) Tarab-Ravski, D.; Stotsky-Oterin, L.; Peer, D. Delivery strategies of RNA therapeutics to leukocytes. *J. Controlled Release* **2022**, *342*, 362−371.

(10) Kranz, L. M.; Diken, M.; Haas, H.; Kreiter, S.; Loquai, C.; Reuter, K. C.; Meng, M.; Fritz, D.; Vascotto, F.; Hefesha, H.; Grunwitz, C.; Vormehr, M.; Hüsemann, Y.; Selmi, A.; Kuhn, A. N.; Buck, J.; Derhovanessian, E.; Rae, R.; Attig, S.; Diekmann, J.; Jabulowsky, R. A.; Heesch, S.; Hassel, J.; Langguth, P.; Grabbe, S.; Huber, C.; Türeci, Ö.; Sahin, U. Systemic RNA delivery to dendritic cells exploits antiviral defence for cancer immunotherapy. *Nature* **2016**, *534*, 396−401.

(11) Cheng, Q.; Wei, T.; Farbiak, L.; Johnson, L. T.; Dilliard, S. A.; Siegwart, D. J. Selective organ targeting (SORT) nanoparticles for tissue-specific mRNA delivery and CRISPR-Cas gene editing. *Nat. Nanotechnol.* **2020**, *15*, 313−320.

(12) McKinlay, C. J.; Vargas, J. R.; Blake, T. R.; Hardy, J. W.; Kanada, M.; Contag, C. H.; Wender, P. A.; Waymouth, R. M. Charge-altering releasable transporters (CARTs) for the delivery and release of mRNA in living animals. *Proc. Natl. Acad. Sci. U.S.A.* **2017**, *114*, E448−E456.

(13) Haabeth, O. A. W.; Blake, T. R.; McKinlay, C. J.; Tveita, A. A.; Sallets, A.; Waymouth, R. M.; Wender, P. A.; Levy, R. Local Delivery of Ox40l, Cd80, and Cd86 mRNA Kindles Global Anticancer Immunity. *Cancer Res.* **2019**, *79*, 1624−1634.

(14) Haabeth, O. A. W.; Blake, T. R.; McKinlay, C. J.; Waymouth, R. M.; Wender, P. A.; Levy, R. mRNA vaccination with charge-altering releasable transporters elicits human T cell responses and cures established tumors in mice. *Proc. Natl. Acad. Sci. U.S.A.* **2018**, *115*, E9153−E9161.

(15) Haabeth, O. A. W.; Lohmeyer, J. J. K.; Sallets, A.; Blake, T. R.; Sagiv-Barfi, I.; Czerwinski, D. K.; McCarthy, B.; Powell, A. E.; Wender, P. A.; Waymouth, R. M.; Levy, R. An mRNA SARS-CoV-2 Vaccine Employing Charge-Altering Releasable Transporters with a TLR-9 Agonist Induces Neutralizing Antibodies and T Cell Memory. *ACS Cent. Sci.* **2021**, *7*, 1191−1204.

(16) Blake, T. R.; Ho, W. C.; Turlington, C. R.; Zang, X.; Huttner, M. A.; Wender, P. A.; Waymouth, R. M. Synthesis and mechanistic investigations of pH-responsive cationic poly(aminoester)s. *Chem. Sci.* **2020**, *11*, 2951−2966.

(17) McKinlay, C. J.; Benner, N. L.; Haabeth, O. A.; Waymouth, R. M.; Wender, P. A. Enhanced mRNA delivery into lymphocytes enabled by lipid-varied libraries of charge-altering releasable transporters. *Proc. Natl. Acad. Sci. U.S.A.* **2018**, *115*, E5859−E5866.

(18) Benner, N. L.; McClellan, R. L.; Turlington, C. R.; Haabeth, O. A. W.; Waymouth, R. M.; Wender, P. A. Oligo(serine ester) Charge-Altering Releasable Transporters: Organocatalytic Ring-Opening Polymerization and their Use for in Vitro and in Vivo mRNA Delivery. *J. Am. Chem. Soc.* **2019**, *141*, 8416−8421.

(19) Loughrey, D.; Dahlman, J. E. Non-liver mRNA Delivery. *Acc. Chem. Res.* **2022**, *55*, 13−23.

(20) Rurik, J. G.; Tombácz, I.; Yadegari, A.; Méndez Fernández, P. O.; Shewale, S. V.; Li, L.; Kimura, T.; Soliman, O. Y.; Papp, T. E.; Tam, Y. K.; Mui, B. L.; Albelda, S. M.; Puré, E.; June, C. H.; Aghajanian, H.; Weissman, D.; Parhiz, H.; Epstein, J. A. CAR T cells produced in vivo to treat cardiac injury. *Science* **2022**, *375*, 91−96.

(21) Volpi, C.; Orabona, C.; Macchiarulo, A.; Bianchi, R.; Puccetti, P.; Grohmann, U. Preclinical discovery and development of fingolimod for the treatment of multiple sclerosis. *Expert Opin. Drug Discovery* **2019**, *14*, 1199−1212.

(22) Yazdi, A.; Ghasemi-Kasman, M.; Javan, M. Possible regenerative effects of fingolimod (FTY720) in multiple sclerosis disease: An overview on remyelination process. *J. Neurosci. Res.* **2020**, *98*, 524−536.

(23) Matloubian, M.; Lo, C. G.; Cinamon, G.; Lesneski, M. J.; Xu, Y.; Brinkmann, V.; Allende, M. L.; Proia, R. L.; Cyster, J. G. Lymphocyte egress from thymus and peripheral lymphoid organs is dependent on S1P receptor 1. *Nature* **2004**, *427*, 355−360.

(24) Chang, W.-T.; Liu, P.-Y.; Wu, S.-N. Actions of FTY720 (Fingolimod), a Sphingosine-1-Phosphate Receptor Modulator, on Delayed-Rectifier K+ Current and Intermediate-Conductance Ca2+-Activated K+ Channel in Jurkat T-Lymphocytes. *Molecules* **2020**, *25*, 4525.

(25) Messias, C. V.; Santana-Van-Vliet, E.; Lemos, J. P.; Moreira, O. C.; Cotta-de-Almeida, V.; Savino, W.; Mendes-da-Cruz, D. A. Sphingosine-1-Phosphate Induces Dose-Dependent Chemotaxis or

https://doi.org/10.1021/acs.biomac.2c00469
Biomacromolecules XXXX, XXX, XXX−XXX

Fugetaxis of T-ALL Blasts through S1P1 Activation. *PLoS One* **2016**, *11*, No. e0148137.
(26) Baer, A.; Colon-Moran, W.; Bhattarai, N. Characterization of the effects of immunomodulatory drug fingolimod (FTY720) on human T cell receptor signaling pathways. *Sci. Rep.* **2018**, *8*, 10910.
(27) Stepanovska, B.; Zivkovic, A.; Enzmann, G.; Tietz, S.; Homann, T.; Kleuser, B.; Engelhardt, B.; Stark, H.; Huwiler, A. Morpholino Analogues of Fingolimod as Novel and Selective $S1P_1$ Ligands with In Vivo Efficacy in a Mouse Model of Experimental Antigen-Induced Encephalomyelitis. *Int. J. Mol. Sci.* **2020**, *21*, 6463.
(28) Imeri, F.; Fallegger, D.; Zivkovic, A.; Schwalm, S.; Enzmann, G.; Blankenbach, K.; Meyer zu Heringdorf, D.; Homann, T.; Kleuser, B.; Pfeilschifter, J.; Engelhardt, B.; Stark, H.; Huwiler, A. Novel oxazolo-oxazole derivatives of FTY720 reduce endothelial cell permeability, immune cell chemotaxis and symptoms of experimental autoimmune encephalomyelitis in mice. *Neuropharmacology* **2014**, *85*, 314−327.
(29) Korin, E.; Bejerano, T.; Cohen, S. GalNAc bio-functionalization of nanoparticles assembled by electrostatic interactions improves siRNA targeting to the liver. *J. Controlled Release* **2017**, *266*, 310−320.
(30) Ong, Z. Y.; Yang, C.; Gao, S. J.; Ke, X.-Y.; Hedrick, J. L.; Yan Yang, Y. Galactose-functionalized cationic polycarbonate diblock copolymer for targeted gene delivery to hepatocytes. *Macromol. Rapid Commun.* **2013**, *34*, 1714−1720.
(31) Chiu, S.-J.; Liu, S.; Perrotti, D.; Marcucci, G.; Lee, R. J. Efficient delivery of a Bcl-2-specific antisense oligodeoxyribonucleotide (G3139) via transferrin receptor-targeted liposomes. *J. Controlled Release* **2006**, *112*, 199−207.
(32) Miettinen, H. M.; Gripentrog, J. M.; Lord, C. I.; Nagy, J. O. CD177-mediated nanoparticle targeting of human and mouse neutrophils. *PLoS One* **2018**, *13*, No. e0200444.
(33) Pham, T. H. M.; Okada, T.; Matloubian, M.; Lo, C. G.; Cyster, J. G. S1P1 receptor signaling overrides retention mediated by G alpha i-coupled receptors to promote T cell egress. *Immunity* **2008**, *28*, 122−133.
(34) Jasiulewicz, A.; Lisowska, K. A.; Pietruczuk, K.; Frąckowiak, J.; Fulop, T.; Witkowski, J. M. Homeostatic "bystander" proliferation of human peripheral blood B cells in response to polyclonal T-cell stimulationin vitro. *Int. Immunol.* **2015**, *27*, 579−588.
(35) Vallé, A.; Zuber, C. E.; Defrance, T.; Djossou, O.; De Rie, M.; Banchereau, J. Activation of human B lymphocytes through CD40 and interleukin 4. *Eur. J. Immunol.* **1989**, *19*, 1463−1467.
(36) Foster, J. B.; Barrett, D. M.; Karikó, K. The Emerging Role of In Vitro-Transcribed mRNA in Adoptive T Cell Immunotherapy. *Mol. Ther.* **2019**, *27*, 747−756.
(37) Bronte, V.; Pittet, M. J. The spleen in local and systemic regulation of immunity. *Immunity* **2013**, *39*, 806−818.
(38) Cerutti, A.; Cols, M.; Puga, I. Marginal zone B cells: virtues of innate-like antibody-producing lymphocytes. *Nat. Rev. Immunol.* **2013**, *13*, 118−132.
(39) Cinamon, G.; Matloubian, M.; Lesneski, M. J.; Xu, Y.; Low, C.; Lu, T.; Proia, R. L.; Cyster, J. G. Sphingosine 1-phosphate receptor 1 promotes B cell localization in the splenic marginal zone. *Nat. Immunol.* **2004**, *5*, 713−720.
(40) Cinamon, G.; Zachariah, M. A.; Lam, O. M.; Foss, F. W., Jr.; Cyster, J. G. Follicular shuttling of marginal zone B cells facilitates antigen transport. *Nat. Immunol.* **2008**, *9*, 54−62.
(41) Ádori, M.; Pedersen, G. K.; Ádori, C.; Erikson, E.; Khoenkhoen, S.; Stark, J. M.; Choi, J. H.; Dosenovic, P.; Karlsson, M. C. I.; Beutler, B.; Karlsson Hedestam, G. B. Altered Marginal Zone B Cell Selection in the Absence of IκBNS. *J. Immunol.* **2018**, *200*, 775−787.
(42) Walzer, T.; Chiossone, L.; Chaix, J.; Calver, A.; Carozzo, C.; Garrigue-Antar, L.; Jacques, Y.; Baratin, M.; Tomasello, E.; Vivier, E. Natural killer cell trafficking in vivo requires a dedicated sphingosine 1-phosphate receptor. *Nat. Immunol.* **2007**, *8*, 1337−1344.
(43) Scott, F. L.; Clemons, B.; Brooks, J.; Brahmachary, E.; Powell, R.; Dedman, H.; Desale, H. G.; Timony, G. A.; Martinborough, E.; Rosen, H.; Roberts, E.; Boehm, M. F.; Peach, R. J. Ozanimod (RPC1063) is a potent sphingosine-1-phosphate receptor-1 (S1P1) and receptor-5 (S1P5) agonist with autoimmune disease-modifying activity. *Br. J. Pharmacol.* **2016**, *173*, 1778−1792.
(44) Attanavanich, K.; Kearney, J. F. Marginal zone, but not follicular B cells, are potent activators of naive CD4 T cells. *J. Immunol.* **2004**, *172*, 803−811.
(45) Marinkovic, D.; Marinkovic, T. Putative role of marginal zone B cells in pathophysiological processes. *Scand. J. Immunol.* **2020**, *92*, No. e12920.
(46) Palm, A.-K. E.; Kleinau, S. Marginal zone B cells: From housekeeping function to autoimmunity? *J. Autoimmun.* **2021**, *119*, 102627.
(47) Pujanauski, L. M.; Janoff, E. N.; McCarter, M. D.; Pelanda, R.; Torres, R. M. Mouse marginal zone B cells harbor specificities similar to human broadly neutralizing HIV antibodies. *Proc. Natl. Acad. Sci. U.S.A.* **2013**, *110*, 1422−1427.
(48) Shimizu, T.; Abu Lila, A. S.; Kawaguchi, Y.; Shimazaki, Y.; Watanabe, Y.; Mima, Y.; Hashimoto, Y.; Okuhira, K.; Storm, G.; Ishima, Y.; Ishida, T. A Novel Platform for Cancer Vaccines: Antigen-Selective Delivery to Splenic Marginal Zone B Cells via Repeated Injections of PEGylated Liposomes. *J. Immunol.* **2018**, *201*, 2969−2976.
(49) Morvan, M. G.; Lanier, L. L. NK cells and cancer: you can teach innate cells new tricks. *Nat. Rev. Cancer* **2016**, *16*, 7−19.
(50) Wilk, A. J.; Weidenbacher, N. L.-B.; Vergara, R.; Haabeth, O. A. W.; Levy, R.; Waymouth, R. M.; Wender, P. A.; Blish, C. A. Charge-altering releasable transporters enable phenotypic manipulation of natural killer cells for cancer immunotherapy. *Blood Adv.* **2020**, *4*, 4244−4255.
(51) Brinkmann, V.; Billich, A.; Baumruker, T.; Heining, P.; Schmouder, R.; Francis, G.; Aradhye, S.; Burtin, P. Fingolimod (FTY720): discovery and development of an oral drug to treat multiple sclerosis. *Nat. Rev. Drug Discovery* **2010**, *9*, 883−897.
(52) Chun, J.; Hartung, H.-P. Mechanism of action of oral fingolimod (FTY720) in multiple sclerosis. *Clin. Neuropharmacol.* **2010**, *33*, 91−101.
(53) Kamphuis, E.; Junt, T.; Waibler, Z.; Forster, R.; Kalinke, U. Type I interferons directly regulate lymphocyte recirculation and cause transient blood lymphopenia. *Blood* **2006**, *108*, 3253−3261.
(54) Kauffman, K. J.; Mir, F. F.; Jhunjhunwala, S.; Kaczmarek, J. C.; Hurtado, J. E.; Yang, J. H.; Webber, M. J.; Kowalski, P. S.; Heartlein, M. W.; DeRosa, F.; Anderson, D. G. Efficacy and immunogenicity of unmodified and pseudouridine-modified mRNA delivered systemically with lipid nanoparticles in vivo. *Biomaterials* **2016**, *109*, 78−87.
(55) Anderson, B. R.; Muramatsu, H.; Nallagatla, S. R.; Bevilacqua, P. C.; Sansing, L. H.; Weissman, D.; Karikó, K. Incorporation of pseudouridine into mRNA enhances translation by diminishing PKR activation. *Nucleic Acids Res.* **2010**, *38*, 5884−5892.
(56) Mandala, S.; Hajdu, R.; Bergstrom, J.; Quackenbush, E.; Xie, J.; Milligan, J.; Thornton, R.; Shei, G.-J.; Card, D.; Keohane, C.; Rosenbach, M.; Hale, J.; Lynch, C. L.; Rupprecht, K.; Parsons, W.; Rosen, H. Alteration of lymphocyte trafficking by sphingosine-1-phosphate receptor agonists. *Science* **2002**, *296*, 346−349.
(57) Morris, M. A.; Gibb, D. R.; Picard, F.; Brinkmann, V.; Straume, M.; Ley, K. Transient T cell accumulation in lymph nodes and sustained lymphopenia in mice treated with FTY720. *Eur. J. Immunol.* **2005**, *35*, 3570−3580.

https://doi.org/10.1021/acs.biomac.2c00469
Biomacromolecules XXXX, XXX, XXX−XXX